Title:
CD47 regulates pro-metastatic phenotypes through an ERK-dependent epithelial-to-mesenchymal transition program in non-small cell lung cancer

Authors:
Asa P.Y. Lau, Lilian G. Zhai, Yin Fang Wu, Kelsie L. Thu

Addresses:
Keenan Research Centre for Biomedical Science, St. Michael's Hospital, Unity Health Toronto
209 Victoria Street, Toronto, ON, Canada, M5B 1T8

Corresponding author:
Kelsie L. Thu
Li Ka Shing Knowledge Institute, 209 Victoria Street, Toronto, ON, Canada M5B 1T8
E-mail: kelsie.thu@unityhealth.to
Phone: 1-416-360-4000 (please do not publish telephone number)

Running title:
CD47 regulation of EMT in lung cancer

Keywords:
CD47, NSCLC, EMT, MAPK signaling, RNA-sequencing

Abbreviations:
NSCLC - non-small cell lung cancer
EMT - epithelial-mesenchymal transition
TSP-1 - thrombospondin-1
KO - knockout
RNP - ribonucleoprotein
CDS - coding sequence
IF - Immunofluorescence
SRB - sulforhodamine B
TCA - trichloroacetic acid
DEG - differentially expressed genes
GSEA - geneset enrichment analyses
MAPK - mitogen-activated protein kinase
FDR - false-discovery rate

Abstract

CD47 is best known for its role in tumor immune evasion; however, studies in diverse cell models indicate that it also has cell-autonomous, tumor-promoting functions which are cell type- and context-specific. Motivated by CD47's prognostic and therapeutic significance and the limited knowledge regarding its roles beyond immune evasion in non-small cell lung cancer (NSCLC), we sought to define the cellular and molecular processes driven by intrinsic CD47 signaling in NSCLC. Transcriptome profiling of CD47 wildtype and knockout NSCLC models implicated its regulation of genes enriched for signatures of epithelial-to-mesenchymal transition (EMT) and MAPK signaling. Functional studies indicated that CD47 does not regulate cell proliferation in NSCLC cells as it does in other cancer types. Instead, we found that CD47 regulates cell adhesion and migration through an ERK-dependent mechanism, validating our transcriptomic findings. Our discoveries reveal a novel role for CD47 in relaying signals through ERK to promote EMT expression programs and pro-metastatic phenotypes in NSCLC. These findings reinforce CD47's therapeutic potential, rationalizing further research to develop CD47 blockade as a multimodal therapy for NSCLC.

1.0 Introduction

Despite global declines in tobacco smoking rates and the implementation of screening programs in developed countries, lung cancer remains the leading cause of cancer-related deaths worldwide [1,2]. Approximately 40% of lung cancer patients are diagnosed with advanced stage disease characterized by tumor metastasis to distant sites [3]. Accordingly, outcomes for lung cancer patients are relatively poor compared to those for other common malignancies, with the 5-year overall survival rate estimated to be 27% [4]. Non-small cell lung cancer (NSCLC) is the most prevalent type of lung cancer. Current treatments include surgery, radiation, chemotherapy, targeted therapy, and/or immunotherapy which are assigned based on tumor stage, histotype, mutation status, and other biomarkers like PD-L1 [5,6]. Over the past decade, immunotherapies that inhibit the immune checkpoint proteins PD-(L)1 and CTLA-4 have shown remarkable efficacy in some NSCLC patients, however, only 30-40% of patients are eligible for these drugs and only 15-20% respond [7,8]. In NSCLC patients who respond to PD-(L)1 blockade, more than 60% develop acquired resistance [9,10]. These statistics indicate that alternative immunotherapies for treating patients ineligible for, or resistant to, current immune checkpoint inhibitors are needed to improve survival rates.

Cluster of differentiation 47, CD47 (also known as integrin associated protein, IAP), is a transmembrane protein often overexpressed on tumor cells that has emerged as a promising immunotherapeutic target in NSCLC and other cancers [11–14]. It is best known for its immunosuppressive function mediated through interactions with its receptor SIRPα, which is expressed on phagocytes like macrophages and dendritic cells. Ligation of CD47 and SIRPα stimulates a signaling cascade that transduces a potent “don’t eat me” signal to inhibit the ability of these cells to perform phagocytosis [14]. As such, cancer cells exploit this checkpoint mechanism to escape phagocytic clearance, suppress anti-tumor immune responses, and evade destruction by the immune system. Discovery of its role in immune evasion led to the development of CD47-targeted immunotherapies. Studies in preclinical models have shown that inhibiting the CD47-SIRPα checkpoint using therapeutic antibodies or fusion proteins (i.e., CD47 blockade) impairs the growth of several tumor types and that these effects are driven by relieving CD47-mediated suppression of phagocytes and their activation of adaptive tumor immunity [15].

Given its promise as an immunotherapeutic target, much research on CD47 in the oncology field has focused on its immunosuppressive function. However, apart from its role in tumor immune escape, CD47 regulates other processes that promote tumor growth and progression [14,16]. These include regulation of autophagy, cell death and survival, angiogenesis, metabolism, and response to stress, which are driven by its interactions with proteins like thrombospondin-1 (TSP-1) and integrins including αvβ3, αIIbβ3, and αβ1 [14,16]. Discoveries of these CD47 functions have been made in diverse physiological and cellular contexts including non-malignant epithelial, endothelial, and smooth muscle cells, as well as cancer models. Findings to date indicate that cell-intrinsic CD47 signaling pathways and their biological effects are pleiotropic and cell type-specific due to differential expression of CD47-interacting proteins in different cells and environments [16]. Thus, studies to decipher CD47 signaling and its cell autonomous effects specifically in lung cancer are necessary to better understand its contributions to lung tumor biology and therapeutic significance.

Investigations of CD47 in NSCLC have determined that it is frequently overexpressed and that high expression is associated with advanced tumor stage, metastasis, and poor survival [11–

13,17]. Functional studies in preclinical models have shown that CD47 inhibition impairs lung tumor growth and progression [18–20], with recent work indicating that combinations of CD47 blockade with EGFR/KRAS/ALK-targeted therapies may be effective treatment strategies for NSCLC [21,22]. Associations between CD47 and cell migration, metastasis and resistance to EGFR-targeted therapy have also been reported in lung cancer [13,20,21,23,24], but the signaling mechanisms underlying CD47's role in these processes are poorly defined. Therefore, we sought to investigate cell-intrinsic CD47 signaling mechanisms and the tumor-promoting phenotypes they influence in NSCLC cells. Using transcriptomic profiling and functional studies in NSCLC cells engineered with and without CD47 loss of function, we discovered that CD47 promotes molecular programs that drive epithelial-to-mesenchymal transition (EMT) and pro-metastatic phenotypes through an ERK-dependent signaling mechanism. Our findings provide new insights into the cell-intrinsic functions of CD47 in NSCLC, and suggest that its therapeutic potential extends beyond its immunosuppressive activity. As such, continued efforts to develop CD47 blockade as a multimodal treatment strategy for NSCLC are warranted.

2.0 Methods

2.1 Cell culture and lentivirus production

Cell lines were grown at 37°C and 5% CO_2 in DMEM or RPMI 1640 media supplemented with 10% fetal bovine serum, 2mM glutamine, and 100U/ml of penicillin-streptomycin. LLC-Luc (LLC; CVCL_4358) was purchased from Promega. NCI-H1299 (H1299; CVCL_0060) was a generous gift from the late Dr. Adi Gazdar. Platinum-E cells were obtained from Cell BioLabs and used to produce lentivirus encoding Cas9, sgRNA, CD47, and ERK2 by co-transfection of transgene expression vectors with psPAX2 and pMD2.G (Addgene #12260, #12259) using Lipofectamine 3000. All cell lines were confirmed to be negative for mycoplasma using a PCR-based assay and were authenticated using short-tandem repeat profiling within the past 2 years.

2.2 Generation of CD47 knockout (KO) lines

CD47 KO lines were generated using CRISPR-Cas9 ribonucleoproteins (RNP) consisting of recombinant Alt-R HiFi S.p. Cas9 nuclease, Alt-R CRISPR-Cas9 tracrRNA, and crRNA targeting CD47 (Integrated DNA Technologies). RNP were delivered to cells using the Neon electroporation system (Thermo Scientific). sgRNA sequences were as follows: hs.sgCD47: AGTGATGCTGTCTCACACAC, and mm.sg.Cd47 TATAGAGCTGAAAAACCGCA. Electroporated cells were clonally expanded and screened for indels within the targeted CD47 coding sequence (CDS) using Sanger sequencing of PCR products spanning the sgRNA cut site (primers in **Table S1**). TIDE analysis was used to deconvolute the indels generated [25]. Loss of CD47 expression was confirmed as described below.

2.3 CD47 and ERK2 overexpression

Mouse and human CD47 CDS were PCR amplified from LLC cDNA and a human Mammalian Gene Collection clone purchased from The Centre for Applied Genomics SPARC cDNA Archive, respectively. The CDS for human ERK2 was a generous gift from Dr. William Lockwood and mouse ERK2 was also amplified from LLC cDNA. Amplified CDS were TOPO cloned into pCR8/GW/TOPO (Invitrogen, #K250020). All primer sequences are listed in **Table S1**. A Gateway LR Clonase recombination reaction (Invitrogen, #11791020) was performed to

insert the CDS into doxycycline(dox)-inducible lentivectors: pInducer20-Blasticidin-Neomycin (Addgene #109334) for mouse or pInducer20-Neomycin for human (Addgene #44012). Cloned CDS were confirmed with Sanger sequencing. Lentivirus was produced as described above and stable lines were selected and maintained in media prepared with tetracycline-free FBS containing 4 ug/mL blasticidin or 0.2 mg/ml neomycin. Dox-induced expression of the transgenes was confirmed as described below.

2.4 Immunofluorescence, immunoblotting, flow cytometry and real-time quantitative PCR

Immunofluorescence (IF) was used to detect CD47 expression in cells fixed with 2% paraformaldehyde using the following antibodies: anti-mouse Cd47 (1:1000, Biolegend #127514), anti-human CD47 (1:1000, Biolegend #323124), anti-goat AF555 (1:1500) and anti-mouse AF488 (1:1500). DNA was stained with DAPI. Western blots were done using the following antibodies on serum-starved cells: mouse CD47 (1:1000, R&D Systems AF1866), human CD47 (1:1000, CST #63000), p44/42 MAPK (Erk1/2) (1:1000, CST #4696S), phospho-p44/42 MAPK (Erk1/2) (1:1000, CST #4370S), Cdc42 (1:1000, CST #2462), pSRC (1:1000, #2101), SRC (1:1000, #2110), Vimentin (1:1000, #5741), N-Cadherin (1:1000, #13116), E-cadherin (1:1000, #3195), GAPDH (1:5000, CST #97166S), Vinculin (CST #13901S). Anti-mouse IRDye 800CW and anti-rabbit IRDye 680RD secondary antibodies were purchased from LiCORbio (1:10,000). Fluorescence imaging of western blots was performed using the LiCOR Odyssey imaging system. For flow cytometry, cultured cells were lifted with TrypLE and washed in FACs buffer (10% BSA in PBS -/- with 2mM EDTA). Cells were stained with DAPI for viability and anti-human CD47 (1:100, Biolegend #323124) or anti-mouse Cd47 (1:100, Biolegend #127514) antibodies. Stained cells were analyzed on a Sony SP6800 Spectral Cytometer or a Cytoflex-LX. FlowJo software was used for quantitation. RT-qPCR to measure gene expression levels was performed using *HPRT1* as the endogenous control and analyzed using the ΔΔCt method. All qPCR primers are listed in **Table S2.**

2.5 RNA-sequencing (RNA-seq)

Total RNA was extracted from cultured LLC WT and CD47 KO cells using the RNeasy Plus Mini Kit (Qiagen) followed by DNAse treatment. RNA integrity was assessed using the 2100 Bioanalyzer (Agilent). Library preparation (NEB Ultra II Directional polyA mRNA) and paired-end sequencing was done at The Centre for Applied Genomics (Toronto, Canada) generating 30-40 million reads per sample on an Illumina Novaseq. Quality control for the raw sequence data was done using FastQC. Trimmomatic was used to trim adapter sequences and filter out low-quality reads [26]. Cleaned reads were aligned to the Mus musculus GRCm39 transcriptome using the STAR aligner [27]. Principal component analysis and differential expression analysis was conducted using the DESeq2 package in R [28]. Genes with an absolute $\log_2$ fold change > 1 and a false-discovery rate (FDR) < 0.05 were considered significantly differentially expressed. Gene set enrichment analysis (GSEA) was performed using ClusterProfiler in R [29] and additional pathway enrichment analyses was done using EnrichR [30].

2.6 Proliferation, and multi-colour competition assays

For proliferation assays, cells were plated at ~10% confluence in a 24-well dish and images were captured every 2 hours over 3-4 days using the BioTek BioSpa live cell imaging

system coupled to a Cytation 5 multimode imaging reader (Agilent). BioTek Gen 5 software was used to calculate percent confluence (i.e., surface area covered by cells) for each well over the course of the experiment. For multi-colour competition assays, LLC and H1299 cells were engineered with stable Cas9 expression using Lenti-Cas9-blast (Addgene #52962). sgRNA targeting AAVS1 (human negative control), LacZ (mouse negative control), or CD47 were cloned into Lenti-Guide-puro-NLS-GFP or LentiGuide-puro-NLS-mCherry (Addgene #185473 and #185474) and transduced into Cas9+ cells. sgRNA sequences are provided in **Table S3**. mCherry+ sgAAVS1 or sgLacZ were mixed 1:1 with GFP + sgCD47/sgAAVS1/sgLacz cells to compare the relative fitness of cells with and without CD47 perturbation. The ratio of GFP+ to mCherry+ cells was measured over multiple passages by flow cytometry.

2.7 Drug dose response assays

Response of cell lines to paclitaxel and cisplatin was evaluated using dose–response assays. Briefly, cells were seeded into 96-well plates and treated with serial dilutions of each drug or DMSO as a control. After 5 days of treatment, cells were fixed with 10% trichloroacetic acid (TCA), stained with sulforhodamine B (SRB), solubilized with 10 mM Tris·HCl, and absorbance at 570nm was quantified on a spectrophotometer. Viability was calculated as the proportion of SRB signal in drug-treated relative to DMSO-treated wells. Dose-response curves were plotted and IC_{50} values were calculated in GraphPad.

2.8 Cell adhesion and scratch migration assays

For adhesion assays, 96-well plates were coated with 1 mg/mL fibronectin (Sigma-Aldrich, F0895) for 30 minutes at room temperature prior to plating cells. Fibronectin was selected as a substrate since CD47 has been shown to mediate binding of reticulocytes and endothelial cells to fibronectin coated surfaces [31,32]. LLC and H1299 cells were seeded onto fibronectin-coated plates and left to adhere at 37 C for 60 minutes. Plates were washed with PBS three times to remove unadhered cells. Adherent cells were fixed in 10% TCA and stained with SRB, which was then solubilized and quantified as absorbance at 570nm on a spectrophotometer (Molecular Devices). Scratch migration assays were done in 24-well plates coated with 1 mg/mL fibronectin. Cells were plated to reach 80-90% confluence 24 hours later. Confluent monolayers were scratched using the BioTek Autoscratch wound making tool. Plates were imaged using the BioTek BioSpa and Cytation 5 live cell imaging system (Agilent) every 2 hours until wound closure. Scratch areas were analyzed using the BioTek Gen 5 software.

2.9 Statistical analysis

The statistical tests used for data analyses are described in the figure legends. All statistics and plots were generated using R and GraphPad Prism software. For cell culture assays and RNA-seq experiments, 3-9 independent biological replicates were analyzed, each with 3-5 technical replicates done to ensure reproducibility of results. T-tests were done on continuous data from independent experimental replicates assumed to be random representative samples from a normally distributed dataset with equal variance. One-sample t-tests were used to compare fold-change data, setting the hypothetical value to 1. All other t-tests were unpaired student's t-tests conducted with two tails. For all statistical tests, $p < 0.05$ was considered significant with

*$p < 0.05$, **$p < 0.01$, ***$p < 0.001$, and ****$p < 0.0001$. All error bars indicate mean ± standard deviation.

3.0 Results

3.1 Establishment of NSCLC models with CD47 loss of function

To investigate cancer cell-intrinsic signaling and phenotypes influenced by CD47, we used CRISPR to engineer murine Lewis lung carcinoma (LLC) and human NCI-H1299 (H1299) NSCLC cell lines lacking the transmembrane and extracellular domains of CD47, which localize CD47 to the plasma membrane and allow it to bind to extracellular ligands (**Fig.1A)**. Sanger sequencing of single cell-derived clonal lines validated the presence of CRISPR-induced indels in the *CD47* gene **(Fig.S1)**. These indels caused frameshifts resulting in truncations of CD47 protein **(Fig.1A)**. Loss of CD47 expression in these knockout (KO) cell lines was validated by quantitative real-time PCR, immunoblotting, flow cytometry, and immunofluorescence (**Fig.1B-I**), confirming their utility for studying CD47-mediated signaling and its associated phenotypic effects in NSCLC cells.

3.2 WT and CD47 KO NSCLC cells exhibit distinct gene expression profiles

We employed a transcriptomic approach to discover how CD47 influences gene expression patterns in NSCLC cells. RNA-seq data was generated for our LLC lines as part of a different study by our group (unpublished). Gene expression analyses of these isogenic models revealed that WT and CD47 KO cells were transcriptionally distinct as they clustered separately in principal component analysis, with CD47 among the genes segregating the principal components (**Fig.2A;Fig.S2**). Differences in the gene expression profiles of WT and KO cells were apparent upon visualizing the 500 most variably expressed genes (**Fig.2B)**. We next performed comparative analyses to discover genes differentially expressed between WT and KO cells for each clone. This identified 4,875 differentially expressed genes (DEGs) in KO clone E3 and 3,567 in KO clone E5 (FDR < 0.05). Comparing these lists revealed 1,842 DEGs common to both clones (**Fig.2C)**. We then separated the DEG lists into up- and downregulated genes, defined as having a $\log_2$ fold-change in expression >1 or <-1 in KO versus WT cells, respectively, and compared them across the clones. This revealed 1,450 DEGs with matching directions in both clones. As expected, CD47 was identified as a top downregulated gene in KO relative to WT cells. These results suggest that CD47 regulates specific gene expression networks in NSCLC.

3.3 CD47 governs an EMT transcription program in lung cancer cells

We proceeded to determine what biological pathways are affected by gene expression changes driven by CD47 KO. We reasoned that genes downregulated in KO cells would be enriched in pathways that promote cell-intrinsic phenotypes governed by CD47. Accordingly, GSEA on DEGs downregulated in CD47 KO cells identified “Epithelial Mesenchymal Transition” (EMT) as the most significant Hallmark pathway enriched in both KO clones (**Fig.2D-E**). GSEA of downregulated DEGs considering Biological Processes annotated in the Gene Ontology knowledgebase revealed several EMT-related processes including “chemotaxis”, “cell-cell adhesion”, “cytokine production”, “cell migration” and “regulation of MAPK cascade” as significantly enriched (**Fig.2F-G)**. Further confirming the positive association between CD47 and EMT, analyses using the EnrichR tool indicated that genes downregulated in CD47 KO cells were

enriched for targets of the EMT-promoting transcription factors, Twist and Prrx2 **(Fig.2H)**. Assessment of the individual DEGs driving enrichment of the cell adhesion, cell migration, and MAPK signaling pathways revealed numerous genes encoding glycoproteins, matricellular proteins, ligands, and growth factors that contribute to the extracellular matrix and promote EMT **(Fig.2I-K)**. These findings indicate for the first time that CD47 influences the transcriptome and positively regulates EMT-associated gene expression signatures in NSCLC cells.

3.4 Loss of CD47 is associated with reduced N-cadherin expression and enhanced chemosensitivity

As an initial step to validate CD47's role in promoting EMT in lung cancer, we assessed established EMT markers in WT and KO NSCLC cells. LLC and H1299 are inherently mesenchymal-like and are commonly used to model metastasis *in vivo [33,34]*. Accordingly, we did not detect E-cadherin in either line (**Fig.3A,E**). We observed a significant decrease in N-cadherin expression in CD47 KO LLC cells and a non-significant trend towards reduced Vimentin expression in one of the two LLC KO clones (**Fig.3B-D**). No significant reproducible changes in N-cadherin or Vimentin expression were observed in H1299 cells, although a trend of reduced N-cadherin expression in KO cells was evident **(Fig.3F-H)**. Since EMT is strongly associated with cancer drug resistance [35], we tested the sensitivity of WT and KO cells to chemotherapies used to treat NSCLC. Although we observed no reproducible differences in response to cisplatin across both KO clones (**Fig.S3**), CD47 KO enhanced the sensitivity of LLC and H1299 cells to paclitaxel, evident by significantly lower IC_{50} values in KO compared to WT lines **(Fig.3J-M)**. These findings of EMT marker expression and drug sensitivity are consistent with CD47 having a pro-EMT function in NSCLC as indicated by our transcriptomic data.

3.5 CD47 KO impairs EMT phenotypes in NSCLC cells

To further assess the intrinsic relevance of CD47 in NSCLC cells and functionally validate our RNA-seq findings, we investigated the impact of CD47 KO on various malignant phenotypes including those characteristic of EMT. We first tested cell proliferation since several studies have reported that CD47 regulates this essential process in other cancer types [16]. However, live cell imaging of LLC and H1299 cells to monitor confluence over time revealed that CD47 KO had no effect on proliferation in either model **(Fig.4A-B)**. To confirm this result, we compared the relative fitness of cells with WT CD47 versus CRISPR-mediated CD47 knockdown using multicolor competition experiments **(Fig.4C)**. We successfully knocked down CD47 using this approach but again observed no difference in the fitness of CD47-deficient and unperturbed control cells over multiple passages **(Fig.4D-I)**. These results indicate CD47 is dispensable for proliferation in NSCLC cells.

Next, we assessed the effects of CD47 KO on cell adhesion and migration, two processes nominated by our transcriptome analyses that are critical for EMT, cancer metastasis, and progression (**Fig.2F-G**). In both LLC and H1299 models, CD47 KO significantly reduced cell adhesion to fibronectin-coated plates **(Fig.5A,B;Fig.S4A,B)**. We used scratch wound assays to determine the effects of CD47 KO on cell migration. Time lapse imaging of cell monolayers after the scratch was applied revealed that LLC cells with CD47 KO had a significantly impaired ability to migrate compared to WT controls (**Fig.5C;Fig.S4C**), consistent with findings in a previous

NSCLC study [13]. This migration defect was also evident in the H1299 model, although one KO clone did not reach statistical significance (**Fig.5D;Fig.S4D**). These studies indicate the EMT-related gene expression signatures we identified as downregulated in CD47 KO cells are associated with corresponding defects in cell adhesion and migration, functionally validating our transcriptomic discoveries. To confirm CD47's role in mediating these phenotypes, we engineered our CD47 KO cells with dox-inducible CD47 expression **(Fig.5E-H)**. Re-constitution of CD47 rescued the migration defect seen in LLC KO cells and enhanced cell adhesion in one KO clone with the same trend in the other **(Fig.5I,K)**; re-expression also rescued KO-associated defects in adhesion and migration in the H1299 model **(Fig.5J,L)**. Collectively, these functional experiments indicate that CD47 promotes the adhesive and migratory abilities of NSCLC cells, consistent with a pro-EMT function.

3.6 CD47 positively regulates MAPK signaling to promote EMT

We next sought to determine how CD47 signaling regulates EMT in NSCLC cells. Studies in epithelial cells, neurons, platelets and/or cancer cells identified SRC and Cdc42 as downstream mediators of CD47 signaling that stimulate pro-migratory phenotypes [16], but we found no evidence that CD47 regulates these effector proteins (**Fig.S5**). Since our RNA-seq analyses implicated the MAPK cascade as a putative downstream effector of CD47 (**Fig.2F,G**), and MAPK signaling is known to drive EMT [36], we hypothesized that CD47 signals through MAPK to induce pro-EMT transcription programs and associated cellular phenotypes. To test this, we evaluated the effects of CD47 KO on MAPK signaling using phospho-ERK as a readout of pathway activity. Consistent with our hypothesis, we found that phospho-ERK was reduced in LLC and H1299 cells with CD47 KO compared to WT controls (**Fig.6A-D)**. Accordingly, we observed that re-expression of CD47 increased phospho-ERK levels in the KO lines for both models **(Fig.6E-H)**. Finally, we investigated whether elevating phospho-ERK expression in CD47-deficient cells also reversed defects in cell adhesion and migration. Using the same doxycycline-inducible system, we found that increasing ERK expression rescued the cell adhesion and migration deficiencies in CD47 KO LLC cells **(Fig.7A,B,E,F)**. In the H1299 model, elevating ERK rescued cell adhesion in both KO clones and enhanced cell migration in one clone with a reproducible trend observed in the other **(Fig.7C,D,G,H)**. These data demonstrate that CD47-mediated regulation of EMT phenotypes is dependent on the MAPK signaling cascade.

4.0 Discussion

In this study, we sought to elucidate the cell-autonomous functions of CD47 and define its effects on intracellular signaling and molecular programs specifically in NSCLC. We discovered for the first time that lung cancer cells with CD47 KO have distinct transcriptional profiles characterized by diminished expression of EMT and MAPK pathway signatures. Our functional studies validated these molecular findings, demonstrating that CD47 positively regulates EMT phenotypes through an ERK-dependent mechanism in NSCLC cells.

CD47 has been shown to regulate several biological processes that contribute to cellular plasticity and tissue homeostasis, many of which are exploited by cancer cells to promote tumor growth and progression [16]. As recently reviewed by Polara et al., these cell-intrinsic CD47

functions include regulation of proliferation, cell death and survival, metabolism, differentiation, motility, autophagy, senescence and stemness. These functions have been characterized in different cell types including non-malignant glial, epithelial, endothelial, immune, and smooth muscle cells, as well as in various cancer models, and are dictated by the proteins CD47 interacts with [16]. For example, CD47 signaling induced by its ligand TSP-1 stimulates proliferation in astrocytoma and glioblastoma cancer cells but suppresses proliferation in endothelial, NK and T cells, demonstrating the cell-type specificity of CD47's effects [37–40]. The context-specific functions of CD47 motivated us to investigate cell-intrinsic signaling and phenotypes regulated by CD47 in NSCLC. We observed that CD47 KO had no effect on cell proliferation in NSCLC models, consistent with observations in CD47-deficient small-cell lung cancer cells [15]. However, we found that CD47 KO impaired NSCLC migration and adhesion, two phenotypes associated with EMT and integral for cancer cell metastasis [41]. Unlike its effects on proliferation, positive regulation of cell migration and adhesion by CD47 appears to be common across cell types with this phenotype evident in erythrocytes, neutrophils, smooth muscle, epithelial, melanoma, ovarian, lymphoma, and colorectal cancer cells [16]. CD47's ability to promote these phenotypes has been attributed to interactions with TSP-1 and/or integrins in some but not all of these cellular contexts [16].

Our findings complement those of a previous study that implicated CD47 in regulating NSCLC invasion and metastasis [13]. Zhao et al. characterized the cellular effects of CD47 using RNA interference (RNAi) and transient CD47 expression in the A549 and NCI-H520 models. Zhao et al. reported that CD47 promotes migration and invasion and has no effect on cell viability, consistent with our findings. This group identified the Rho GTPase and well-established EMT mediator, Cdc42 [42], as a downstream effector of CD47's regulation of these phenotypes. We observed no change in Cdc42 expression upon CD47 KO in LLC and H1299 cells, suggesting Cdc42 may not be a generalizable mediator of EMT downstream of CD47 in NSCLC. Zhao et al. also found that perturbing CD47 did not alter expression of the canonical EMT markers E-cadherin, N-cadherin, Snail or Slug, leading them to conclude that CD47 does not regulate EMT. However, while we could not detect expression of E-cadherin or Snail/Slug (data not shown) in our models, we observed reduced N-cadherin expression in LLC and H1299 cells with CD47 KO. Additionally, our transcriptomic data strongly implicated CD47 in EMT regulation. We suspect that our differing conclusions regarding CD47's role in EMT in NSCLC could reflect model-specific differences and/or differences in the experimental approaches used. With respect to the former, a recent study reported that tumors leverage different pathways to drive EMT, with cancer cells adopting either embryonic- or adult-like programs regulated by distinct transcription factors [43]. Indeed, our RNA-seq findings implicated PRRX2 and TWIST1 as putative transcription factors driving EMT and pro-metastatic phenotypes downstream of CD47 in NSCLC cells, consistent with the embryonic-like EMT trajectory [43].

Our transcriptomic profiling to define molecular programs underlying CD47's regulation of malignant phenotypes presents a significant advance upon previous work in lung and other cancers. Ours is one of few studies to perform RNA-seq on cancer cells with CD47 LOF to understand its influence on cellular programming, and the first to do so in cancer cells engineered with complete CD47 KO. Dong et al. performed RNA-seq on 8505C thyroid cancer cells to

investigate correlations between CD47 and IFT57's effects on the transcriptome [44]. Using EnrichR to perform enrichment analysis of the genes they identified as significantly downregulated upon CD47 knockdown identified "Epithelial Mesenchymal Transition" as the second most significant hallmark pathway enriched (not shown). In a different study, the same group derived gene expression profiles for triple negative breast cancer cells treated with the CD47 function-blocking agents, SIRPα-Fc fusion protein or anti-CD47 monoclonal antibody CC-90002 [45]. Although "TNFA_SIGNALING_VIA_NFKB", "Inflammatory response", and "IL6_JAK_STAT3_SIGNALING" were the most significant pathway hits in their analyses, genes downregulated upon CD47 blockade were also significantly enriched for the hallmark EMT pathway. Hu et al. characterized transcriptomes of colon cancer cell lines, DLD1 and HCT8, engineered with CD47 overexpression and found that CD47 positively regulates MAPK signaling and metabolic pathways to promote cell migration and metastasis [46]. Their work also implicated CD47 in regulating cell adhesion and extracellular matrix interactions. Therefore, data from each of these studies implicates CD47 in EMT, suggesting that CD47-mediated regulation of pro-EMT transcription programs is conserved across multiple cancer types.

EMT is a reversible biological process that transforms cells from an epithelial to mesenchymal state that bestows them with motility and invasive capabilities [41]. In physiological conditions, cells undergo EMT to facilitate embryonic development and tissue regeneration but cancer cells co-opt EMT to support stemness, metastasis, and resistance to therapy, all of which drive tumor progression [41,47]. Associations between CD47 expression and EMT markers have been reported in multiple cancers including colorectal, prostate, and triple negative breast cancers [48–50]. Corroborating these correlative findings, functional studies have demonstrated that CD47 positively regulates EMT in ovarian cancer, oral squamous cell carcinoma, and hepatocellular carcinoma models [51–53]. Interestingly, a breast cancer study identified CD47 as a target of the canonical pro-EMT transcription factors, ZEB1 and SNAIL [54]. A later study identified CD47 as a target of ZEB1 in a murine model of Kras-driven lung adenocarcinoma [55]. This group reported that CD47 was expressed on invading lung cancer cells and reprogrammed tumor associated macrophages to protect invading cancer cells from immune destruction [55]. Thus, current evidence indicates CD47 both induces cancer EMT and is itself induced by EMT, suggesting CD47 may be an effector of a positive feedback mechanism that reinforces EMT programs; however, mechanistic studies are required to investigate this supposition.

Our data indicated that CD47 promotes EMT-associated phenotypes through an ERK-dependent mechanism. CD47 has previously been described as an upstream regulator of several signal transduction proteins, including SRC, FAK, PI3K, BNIP3, PLCγ1, Cdc42, BECN1, and ERK, which regulate a plethora of cellular functions [16]. CD47's regulation of MAPK signaling in NSCLC is consistent with studies that identified CD47 as a positive regulator of ERK in colorectal cancer, meningioma, and craniopharyngioma models, suggesting CD47-mediated regulation of MAPK signaling is a ubiquitous mechanism in cancer cells [46,56,57]. In contrast, stimulation of CD47 with the TSP-1 derived peptide, 4N1K, diminished phospho-ERK expression and chemotaxis in smooth muscle cells, further highlighting the context-specific nature of CD47 signaling and its phenotypic effects [58]. Another study reported that ERK signaling induces CD47 expression in melanoma models [59]. This aligns with findings from recent studies that identified

the two most prevalent oncogenic drivers in NSCLC, EGFR and KRAS, as positive regulators of CD47 expression [22,60]. In EGFR-driven tumors, CD47 expression was attributed to constitutive activation of the downstream transcription factors c-Myc and NF-κB, as well as CD47 stabilization by SRC-mediated phosphorylation which prevents its degradation [22]. In the context of KRAS, PI3K-STAT3 signaling was found to upregulate CD47 expression by relieving its suppression by miR-34a [60]. These studies and our own suggest a feed-forward mechanism to amplify ERK signaling and CD47 expression may exist in NSCLC cells.

Our discoveries nominate a putative mechanism to explain CD47's involvement in NSCLC metastasis involving activation of MAPK signaling and downstream transcription of EMT-related gene expression signatures. Several studies have reported that high CD47 expression is associated with poor prognosis and the incidence of metastasis in NSCLC patients [11–14], indicating the clinical manifestation of the cell and molecular programs we uncovered in preclinical models. Furthermore, they highlight the potential for CD47 inhibition to antagonize NSCLC metastasis, a major contributor to tumor progression and patient mortality. CD47's ability to promote oncogenic signaling pathways, drive tumor immune escape, and facilitate EMT-associated drug resistance and cancer cell dissemination, highlights the potential for CD47 blockade to be an effective multimodal therapeutic strategy in lung cancer, particularly for EGFR-driven tumors which are enriched for CD47-positivity and refractory to PD-1 blockade [11,12,61]. Numerous agents that disrupt CD47-SIRPα interactions have demonstrated promising anti-cancer effects in preclinical tumor models [13,62,63] but their efficacy in clinical trials has been limited by on-target, off-tumor toxicities [64]. This highlights the need for alternative ways to administer CD47 blockade to realize its therapeutic potential, including methods to deliver drugs preferentially to tumor tissues [65] and combination approaches to prime tumors for response to CD47 inhibition [14]. Our finding that CD47 induces phospho-ERK provides a biological rationale for combining CD47 blockade with EGFR/KRAS-targeted therapies to abrogate residual ERK activity and immune escape following EGFR/KRAS inhibition. Accordingly, the combination of EGFR/KRAS- and CD47-targeted therapies was recently shown to exert synergistic effects in preclinical NSCLC models [21]. This warrants continued research to identify strategies to overcome challenges associated with the current modes of delivering CD47 blockade in the clinic. The improved understanding of CD47's cell-intrinsic functions in NSCLC that our work has provided indicates that clinical translation of CD47 inhibitors could greatly benefit patients due to CD47's multi-faceted contributions to tumor progression.

We conducted our studies in cell models representing human and murine NSCLC driven by Ras-family oncogenes (NRAS in H1299 and Kras/Nras in LLC). Our use of clonally-derived CD47 KO lines ensured complete CD47 LOF was achieved in the cells studied. It is possible that CD47 signaling and the phenotypes it controls differ in lung cancers with distinct proteome expression patterns, genetic drivers, and histologies. This could explain differences seen in specific phenotypes in our study and other NSCLC studies (eg. Cdc42 as a CD47 effector protein and CD47's effect on cisplatin sensitivity). Characterizing CD47 signaling in cell models enabled us to study cell-autonomous CD47 signaling in a controlled environment; however, future *in vivo* studies are warranted to define how cell-intrinsic CD47 signaling is influenced by extrinsic cues from immune and other stromal cells in the tumor microenvironment. Although we identified ERK

as a downstream effector of CD47 signaling in NSCLC cells, the ligands that stimulate CD47 as well as the effectors up- and downstream of ERK remain to be defined. Thus, while we uncovered new insights into CD47's regulation of EMT and pro-metastatic phenotypes through an ERK-dependent mechanism in NSCLC, additional studies are needed to further decipher the CD47 interactome and its downstream signaling effectors in NSCLC cells.

5.0 Conclusion

Our work advances knowledge of CD47's cell-intrinsic functions in the context of NSCLC. We discovered that CD47 regulates MAPK signaling and EMT to stimulate tumor-promoting phenotypes, demonstrating that it functions as more than just an immunosuppressive signal. These findings deepen the fundamental understanding of how CD47 contributes to lung cancer biology and highlight the multimodal potential for CD47-targeted therapy to benefit NSCLC patients. As such, further research to develop improved therapeutic agents for delivering CD47 blockade with better toxicity profiles and anti-tumor activities is warranted.

6.0 Data Accessibility

RNA-seq data will be deposited within the Gene Expression Omnibus upon publication.

7.0 Author Contributions

AL and KLT were responsible for study conception, experimental design, and manuscript preparation. AL conducted experiments with assistance from LZ, YFW, and KLT. AL performed data analysis. All authors made significant contributions and critically reviewed the manuscript.

8.0 Acknowledgements

The authors are grateful to Drs. Katalin Szaszi, Andras Kapus, Shannon Dunn, and Sunit Das for helpful scientific discussions and experimental suggestions. The authors thank UHT core facility scientists, Drs. Caterina Di Ciano Oliveira, Xiaofeng Lu, Pamela Plant, and Monika Lodyga for their technical support.

9.0 Funding Sources and COI

This research was funded by Unity Health Toronto (UHT), Cancer Research Society (#24513), JP Bickell Foundation Research Grant, Canada Research Chairs program (#233198). AL was supported by scholarships from the Canadian Institutes of Health Research, Government of Ontario, UHT Research Training Centre, and University of Toronto's Laboratory Medicine and Pathobiology Department. LZ was supported by a scholarship from the University of Toronto's Laboratory Medicine and Pathobiology Department. The authors have no conflicts of interest to disclose.

10.0 References

1. Sung H, Ferlay J, Siegel RL, Laversanne M, Soerjomataram I, Jemal A, et al. Global Cancer Statistics 2020: GLOBOCAN Estimates of Incidence and Mortality Worldwide for 36 Cancers in 185 Countries. CA Cancer J Clin. 2021;71: 209–249.
2. Tammemägi MC, Darling GE, Schmidt H, Walker MJ, Langer D, Leung YW, et al. Risk-based lung cancer screening performance in a universal healthcare setting. Nat Med. 2024;30: 1054–1064.
3. Morgensztern D, Ng SH, Gao F, Govindan R. Trends in stage distribution for patients with non-small cell lung cancer: a National Cancer Database survey. J Thorac Oncol. 2010;5: 29–33.
4. Siegel RL, Kratzer TB, Giaquinto AN, Sung H, Jemal A. Cancer statistics, 2025. CA Cancer J Clin. 2025;75: 10–45.
5. Zhang Y, Vaccarella S, Morgan E, Li M, Etxeberria J, Chokunonga E, et al. Global variations in lung cancer incidence by histological subtype in 2020: a population-based study. Lancet Oncol. 2023;24: 1206–1218.
6. Guo Q, Liu L, Chen Z, Fan Y, Zhou Y, Yuan Z, et al. Current treatments for non-small cell lung cancer. Front Oncol. 2022;12: 945102.
7. Haslam A, Gill J, Prasad V. Estimation of the Percentage of US Patients With Cancer Who Are Eligible for Immune Checkpoint Inhibitor Drugs. JAMA Netw Open. 2020;3: e200423.
8. Haslam A, Prasad V. Estimation of the Percentage of US Patients With Cancer Who Are Eligible for and Respond to Checkpoint Inhibitor Immunotherapy Drugs. JAMA Netw Open. 2019;2: e192535.
9. Memon D, Schoenfeld AJ, Ye D, Fromm G, Rizvi H, Zhang X, et al. Clinical and molecular features of acquired resistance to immunotherapy in non-small cell lung cancer. Cancer Cell. 2024;42: 209–224.e9.
10. Boyero L, Sánchez-Gastaldo A, Alonso M, Noguera-Uclés JF, Molina-Pinelo S, Bernabé-Caro R. Primary and acquired resistance to immunotherapy in lung cancer: Unveiling the mechanisms underlying of immune checkpoint blockade therapy. Cancers (Basel). 2020;12: 3729.
11. Arrieta O, Aviles-Salas A, Orozco-Morales M, Hernández-Pedro N, Cardona AF, Cabrera-Miranda L, et al. Association between CD47 expression, clinical characteristics and prognosis in patients with advanced non-small cell lung cancer. Cancer Med. 2020;9: 2390–2402.
12. Xu Y, Li J, Tong B, Chen M, Liu X, Zhong W, et al. Positive tumour CD47 expression is an independent prognostic factor for recurrence in resected non-small cell lung cancer. ESMO Open. 2020;5. doi:10.1136/esmoopen-2020-000823
13. Zhao H, Wang J, Kong X, Li E, Liu Y, Du X, et al. CD47 Promotes Tumor Invasion and Metastasis in Non-small Cell Lung Cancer. Sci Rep. 2016;6: 29719.
14. Lau APY, Khavkine Binstock SS, Thu KL. CD47: The Next Frontier in Immune Checkpoint Blockade for Non-Small Cell Lung Cancer. Cancers . 2023;15. doi:10.3390/cancers15215229
15. Weiskopf K, Jahchan NS, Schnorr PJ, Cristea S, Ring AM, Maute RL, et al. CD47-blocking immunotherapies stimulate macrophage-mediated destruction of small-cell lung cancer. J Clin Invest. 2016;126: 2610–2620.
16. Polara R, Ganesan R, Pitson SM, Robinson N. Cell autonomous functions of CD47 in regulating cellular plasticity and metabolic plasticity. Cell Death Differ. 2024;31: 1255–1266.
17. Fu F, Zhang Y, Gao Z, Zhao Y, Wen Z, Han H, et al. Combination of CD47 and CD68 expression predicts survival in eastern-Asian patients with non-small cell lung cancer. J Cancer Res Clin Oncol. 2021;147: 739–747.
18. Liu L, Zhang L, Yang L, Li H, Li R, Yu J, et al. Anti-CD47 Antibody As a Targeted

Therapeutic Agent for Human Lung Cancer and Cancer Stem Cells. Front Immunol. 2017;8: 404.
19. Zhang X, Wang Y, Fan J, Chen W, Luan J, Mei X, et al. Blocking CD47 efficiently potentiated therapeutic effects of anti-angiogenic therapy in non-small cell lung cancer. J Immunother Cancer. 2019;7: 346.
20. Nigro A, Ricciardi L, Salvato I, Sabbatino F, Vitale M, Crescenzi MA, et al. Enhanced Expression of CD47 Is Associated With Off-Target Resistance to Tyrosine Kinase Inhibitor Gefitinib in NSCLC. Front Immunol. 2019;10: 3135.
21. Vaccaro K, Allen J, Whitfield TW, Maoz A, Reeves S, Velarde J, et al. Targeted therapies prime oncogene-driven lung cancers for macrophage-mediated destruction. J Clin Invest. 2024. doi:10.1172/JCI169315
22. Hu L-Y, Zhuang W-T, Chen M-J, Liao J, Wu D-F, Zhang Y-X, et al. EGFR oncogenic mutations in NSCLC impair macrophage phagocytosis and mediate innate immune evasion through up-regulation of CD47. J Thorac Oncol. 2024;19: 1186–1200.
23. Qu S, Jiao Z, Lu G, Xu J, Yao B, Wang T, et al. Human lung adenocarcinoma CD47 is upregulated by interferon-γ and promotes tumor metastasis. Mol Ther Oncolytics. 2022;25: 276–287.
24. Lu J, Li J, Lin Z, Li H, Lou L, Ding W, et al. Reprogramming of TAMs via the STAT3/CD47-SIRPα axis promotes acquired resistance to EGFR-TKIs in lung cancer. Cancer Lett. 2023;564: 216205.
25. Brinkman EK, Chen T, Amendola M, van Steensel B. Easy quantitative assessment of genome editing by sequence trace decomposition. Nucleic Acids Res. 2014;42: e168.
26. Bolger AM, Lohse M, Usadel B. Trimmomatic: a flexible trimmer for Illumina sequence data. Bioinformatics. 2014;30: 2114–2120.
27. Dobin A, Davis CA, Schlesinger F, Drenkow J, Zaleski C, Jha S, et al. STAR: ultrafast universal RNA-seq aligner. Bioinformatics. 2013;29: 15–21.
28. Love MI, Huber W, Anders S. Moderated estimation of fold change and dispersion for RNA-seq data with DESeq2. Genome Biol. 2014;15: 550.
29. Yu G, Wang L-G, Han Y, He Q-Y. clusterProfiler: an R package for comparing biological themes among gene clusters. OMICS. 2012;16: 284–287.
30. Xie Z, Bailey A, Kuleshov MV, Clarke DJB, Evangelista JE, Jenkins SL, et al. Gene set knowledge discovery with Enrichr. Curr Protoc. 2021;1: e90.
31. Brittain JE, Han J, Ataga KI, Orringer EP, Parise LV. Mechanism of CD47-induced alpha4beta1 integrin activation and adhesion in sickle reticulocytes. J Biol Chem. 2004;279: 42393–42402.
32. Schwartz MA, Brown EJ, Fazeli B. A 50-kDa integrin-associated protein is required for integrin-regulated calcium entry in endothelial cells. J Biol Chem. 1993;268: 19931–19934.
33. Kellar A, Egan C, Morris D. Preclinical Murine models for lung cancer: Clinical trial applications. Biomed Res Int. 2015;2015: 621324.
34. Singla AK, Downey CM, Bebb GD, Jirik FR. Characterization of a murine model of metastatic human non-small cell lung cancer and effect of CXCR4 inhibition on the growth of metastases. Oncoscience. 2015;2: 263–271.
35. Shibue T, Weinberg RA. EMT, CSCs, and drug resistance: the mechanistic link and clinical implications. Nat Rev Clin Oncol. 2017;14: 611–629.
36. Gonzalez DM, Medici D. Signaling mechanisms of the epithelial-mesenchymal transition. Sci Signal. 2014;7: re8.
37. Gao Q, Chen K, Gao L, Zheng Y, Yang Y-G. Thrombospondin-1 signaling through CD47 inhibits cell cycle progression and induces senescence in endothelial cells. Cell Death Dis. 2016;7: e2368.
38. Kaur S, Soto-Pantoja DR, Stein EV, Liu C, Elkahloun AG, Pendrak ML, et al. Thrombospondin-1 signaling through CD47 inhibits self-renewal by regulating c-Myc and

other stem cell transcription factors. Sci Rep. 2013;3: 1673.
39. Nath PR, Pal-Nath D, Mandal A, Cam MC, Schwartz AL, Roberts DD. Natural killer cell recruitment and activation are regulated by CD47 expression in the tumor microenvironment. Cancer Immunol Res. 2019;7: 1547–1561.
40. Kaur S, Chang T, Singh SP, Lim L, Mannan P, Garfield SH, et al. CD47 signaling regulates the immunosuppressive activity of VEGF in T cells. J Immunol. 2014;193: 3914–3924.
41. Huang Y, Hong W, Wei X. The molecular mechanisms and therapeutic strategies of EMT in tumor progression and metastasis. J Hematol Oncol. 2022;15: 129.
42. Stengel K, Zheng Y. Cdc42 in oncogenic transformation, invasion, and tumorigenesis. Cell Signal. 2011;23: 1415–1423.
43. Youssef KK, Narwade N, Arcas A, Marquez-Galera A, Jiménez-Castaño R, Lopez-Blau C, et al. Two distinct epithelial-to-mesenchymal transition programs control invasion and inflammation in segregated tumor cell populations. Nat Cancer. 2024;5: 1660–1680.
44. Dong K, Nihal R, Meyer TJ, Singh SP, Kaur S, Roberts DD. CD47 and IFT57 are colinear genes that are highly coexpressed in most cancers and exhibit parallel cancer-specific correlations with survival. Int J Mol Sci. 2024;25: 8956.
45. Kaur S, Reginauld B, Razjooyan S, Phi T, Singh SP, Meyer TJ, et al. Effects of a humanized CD47 antibody and recombinant SIRPα proteins on triple negative breast carcinoma stem cells. Front Cell Dev Biol. 2024;12: 1356421.
46. Hu T, Liu H, Liang Z, Wang F, Zhou C, Zheng X, et al. Tumor-intrinsic CD47 signal regulates glycolysis and promotes colorectal cancer cell growth and metastasis. Theranostics. 2020;10: 4056–4072.
47. Dela Cruz MCP, Medina PMB. Epithelial-mesenchymal transition (EMT) and its role in acquired epidermal growth factor receptor-tyrosine kinase inhibitor (EGFR-TKI) chemoresistance in non-small cell lung cancer (NSCLC). Cancer Pathog Ther. 2025;3: 215–225.
48. Fujiwara-Tani R, Sasaki T, Ohmori H, Luo Y, Goto K, Nishiguchi Y, et al. Concurrent expression of CD47 and CD44 in colorectal cancer promotes malignancy. Pathobiology. 2019;86: 182–189.
49. Yuan J, Shi X, Chen C, He H, Liu L, Wu J, et al. High expression of CD47 in triple negative breast cancer is associated with epithelial-mesenchymal transition and poor prognosis. Oncol Lett. 2019;18: 3249–3255.
50. Feng D, Shi X, Xiong Q, Zhang F, Li D, Yang L. A gene prognostic index associated with epithelial-mesenchymal transition predicting biochemical recurrence and tumor chemoresistance for prostate cancer. Front Oncol. 2021;11: 805571.
51. Li Y, Lu S, Xu Y, Qiu C, Jin C, Wang Y, et al. Overexpression of CD47 predicts poor prognosis and promotes cancer cell invasion in high-grade serous ovarian carcinoma. Am J Transl Res. 2017;9: 2901–2910.
52. Pai S, Bamodu OA, Lin Y-K, Lin C-S, Chu P-Y, Chien M-H, et al. CD47-SIRPα signaling induces epithelial-mesenchymal transition and cancer stemness and links to a poor prognosis in patients with oral squamous cell carcinoma. Cells. 2019;8: 1658.
53. Fan Z, Gao Y, Zhang W, Yang G, Liu P, Xu L, et al. METTL3/IGF2BP1/CD47 contributes to the sublethal heat treatment induced mesenchymal transition in HCC. Biochem Biophys Res Commun. 2021;546: 169–177.
54. Noman MZ, Van Moer K, Marani V, Gemmill RM, Tranchevent L-C, Azuaje F, et al. CD47 is a direct target of SNAI1 and ZEB1 and its blockade activates the phagocytosis of breast cancer cells undergoing EMT. Oncoimmunology. 2018;7: e1345415.
55. Guo Y, Lu X, Chen Y, Rendon B, Mitchell RA, Cuatrecasas M, et al. Zeb1 induces immune checkpoints to form an immunosuppressive envelope around invading cancer cells. Sci Adv. 2021;7: eabd7455.
56. Liu X, Zhang H, Wang C, Li Z, Zhu Q, Feng Y, et al. Tumor-selective blockade of CD47

signaling with CD47 antibody for enhanced anti-tumor activity in malignant meningioma. Curr Neuropharmacol. 2023;21: 2159–2173.
57. Zhang H, Wang C, Fan J, Zhu Q, Feng Y, Pan J, et al. CD47 promotes the proliferation and migration of adamantinomatous craniopharyngioma cells by activating the MAPK/ERK pathway, and CD47 blockade facilitates microglia-mediated phagocytosis. Neuropathol Appl Neurobiol. 2022;48: e12795.
58. Wang XQ, Lindberg FP, Frazier WA. Integrin-associated protein stimulates alpha2beta1-dependent chemotaxis via Gi-mediated inhibition of adenylate cyclase and extracellular-regulated kinases. J Cell Biol. 1999;147: 389–400.
59. Liu F, Jiang CC, Yan XG, Tseng H-Y, Wang CY, Zhang YY, et al. BRAF/MEK inhibitors promote CD47 expression that is reversible by ERK inhibition in melanoma. Oncotarget. 2017;8: 69477–69492.
60. Hu H, Cheng R, Wang Y, Wang X, Wu J, Kong Y, et al. Oncogenic KRAS signaling drives evasion of innate immune surveillance in lung adenocarcinoma by activating CD47. J Clin Invest. 2023;133. doi:10.1172/JCI153470
61. Doroshow DB, Sanmamed MF, Hastings K, Politi K, Rimm DL, Chen L, et al. Immunotherapy in Non-Small Cell Lung Cancer: Facts and Hopes. Clin Cancer Res. 2019;25: 4592–4602.
62. Yu W-B, Chen Y-C, Huang C-Y, Ye Z-H, Shi W, Zhu H, et al. CD47 blockade improves the therapeutic effect of osimertinib in non-small cell lung cancer. Front Med. 2023;17: 105–118.
63. Wang Y, Zhao C, Liu Y, Wang C, Jiang H, Hu Y, et al. Recent advances of tumor therapy based on the CD47-SIRPα axis. Mol Pharm. 2022;19: 1273–1293.
64. Jiang C, Sun H, Jiang Z, Tian W, Cang S, Yu J. Targeting the CD47/SIRPα pathway in malignancies: recent progress, difficulties and future perspectives. Front Oncol. 2024;14: 1378647.
65. Hoshi R, Gorospe KA, Labouta HI, Azad T, Lee WL, Thu KL. Alternative strategies for delivering immunotherapeutics targeting the PD-1/PD-L1 immune checkpoint in cancer. Pharmaceutics. 2024;16: 1181.

Figure Legends

Figure 1. Generation of isogenic CD47 KO NSCLC models. A) Schematic representation of LLC and H1299 lines engineered with deletion of the C-terminal half of CD47, which encodes its transmembrane and cytoplasmic tail domains. The signal peptide (light blue), transmembrane domains (grey), extra/intracellular domains (dark blue), and cytoplasmic tail (purple) are indicated. Confirmation of CD47 KO by qPCR **(B-C)**, immunoblotting **(D-E)**, flow cytometry **(F-G),** and immunofluorescence **(H-I)**.

Figure 2. CD47 KO cells exhibit transcriptomic changes associated with downregulation of EMT pathways. A) Principal component analysis indicating dissimilarity in transcriptomes of LLC WT and CD47 KO cells. **B)** Heatmap of the 500 most variably expressed genes in LLC cells. CD47 is one of the most significantly downregulated genes in CD47 KO cells and is represented in this heatmap. **C)** Statistically significant DEGs common to both CD47 KO lines. **D-G)** GSEA results indicating gene sets enriched for downregulated DEGs in CD47 KO cells. **D-E)** MSigDB Hallmark pathways and **F-G)** Gene Ontology: Biological Processes (GO:BP). **H)** Top ARCHS4 Transcription Factor gene sets enriched for downregulated DEGs identified using EnrichR. **I-K)** Genes contributing to the Cell-Cell Adhesion, Cell Migration, and MAPK Signaling processes enriched for DEGs that are downregulated in CD47 KO cells. The colour scale indicates the average $\log_2$ fold change in expression across both CD47 KO clones relative to WT cells.

Figure 3. CD47 KO reduces N-cadherin expression and sensitizes lung cancer cells to paclitaxel. A,B) Immunoblotting for EMT markers, E-cadherin, N-cadherin, and Vimentin in the LLC model. **C,D)** Quantitation of EMT marker expression across replicate experiments in LLC cells. **E,F)** EMT marker expression in the H1299 model. **G,H)** Quantitation of EMT marker expression in H1299 cells. One-sample t-tests were used to compare the fold-change in expression between WT and KO cells. **I-L)** Dose response curves and IC_{50} values indicating the response of LLC and H1299 lines to paclitaxel. Paclitaxel treatments were done using a maximum dose of 500nM and 2-fold serial dilutions. IC_{50} values were compared between WT and CD47 KO cells using a two-tailed student's t-test.

Figure 4. CD47 KO does not affect lung cancer cell proliferation or fitness. A-B) Imaging-based proliferation assay monitoring cell confluence over 48 or 92 hours. Percent confluence indicates the fraction of well area covered by cells. Comparisons of confluencies between WT and CD47 KO cells were done using two-tailed student's t-test with multiple testing correction across all timepoints for LLC and H1299. All t-tests between WT and KO cells were non-significant. **C)** Schematic representation of the multi-colour competition assays. **D-E)** Western blots confirming CRISPR-mediated loss of CD47 expression in LLC and H1299 Cas9+ lines. Cas9-expressing cells were transduced with mCherry (mCH) or GFP lentivectors to express control sgRNA targeting LacZ (for mouse) or AAVS1 (AV, for human), or sgRNA targeting CD47 (CD47-1, CD47-2). **F-G)** Loss of CD47 surface expression confirmed by flow cytometry. **H-I)** Competition assay results indicating the relative fitness of cells with wildtype (sgLacZ, sgAV) *CD47* versus cells with genetically disrupted *CD47* (sgCD47). "ns" indicates t-test results for

comparing GFP+ ratios between the different cell mixtures at the final passage. Data are representative of three independent experiments for each model.

Figure 5. CD47 KO impairs lung cancer adhesion and migration. A-B) Results for cell adhesion assays in the LLC and H1299 models one hour after cell seeding. Cell density was quantified based on SRB staining. **C-D)** Wound healing assays to measure cell migration after scratching a confluent monolayer. Wound width was quantified at two timepoints after the scratch and normalized to the initial wound width. Asterisks shown indicate statistical significance at assay endpoints. Data presented for cell adhesion assays are representative of 3 independent experiments. Data for migration assays are representative of 3-4 independent experiments. **E-F)** Western blots confirming CD47 reconstitution in LLC and H1299 cells with CD47 KO. CD47 expression was induced by treating LLC cells with 500 ng/mL and H1299 with 100 ng/mL of doxycycline (Dox) for 24hrs. **G-H)** Flow cytometry confirmation of surface level CD47 expression after Dox induction in the CD47 KO lines. **I-J)** Results for adhesion assays in CD47-deficient LLC and H1299 cells with and without Dox-induced re-expression of CD47. **K-L)** Migration assay results for the same cells in I,J. Adhesion assays results in I,J are representative of 3 independent experiments. Migration assay results in K,L are representative of 3 independent experiments. Comparisons between groups were done using two-tailed t-tests.

Figure 6. CD47 KO reduces MAPK signaling in lung cancer cells. A-D) Western blots and quantitation for phospho-ERK (pERK) expression in WT versus CD47 KO cells under basal conditions. pERK expression is presented as a fold-change relative to total ERK expression and compared across groups using a one-sample t-test. **E-H)** Western blots and quantitation of CD47 and pERK in LLC and H1299 CD47 KO cells with and without 24-48h of Dox treatment at 500 ng/ml (LLC) or 100 ng/ml (H1299) to induce CD47 expression.

Figure 7. CD47-mediated regulation of cell adhesion and migration is ERK dependent. A-D) Immunoblots and quantitation confirming phospho-ERK (pERK) upregulation in LLC and H1299 WT and CD47 KO cells expressing a Dox-inducible ERK2 construct treated with and without 500 ng/ml (LLC) or 100ng/ml (H1299) Dox for 24-48h. pERK expression is normalized to Vinculin (Vinc) since Dox treatment induces total ERK and fold-changes in pERK expression were compared with one-sample t-tests. **E-H)** Results for adhesion and migration assays in the same ERK-inducible LLC and H1299 cells pre-treated with or without 500 ng/ml (LLC) or 100ng/ml (H1299) Dox for 24-48h. Asterisks shown indicate statistical significance for two-tailed t-tests. Data presented are representative of 3 (LLC) and 3 (H1299) replicate experiments.

Figure. 1

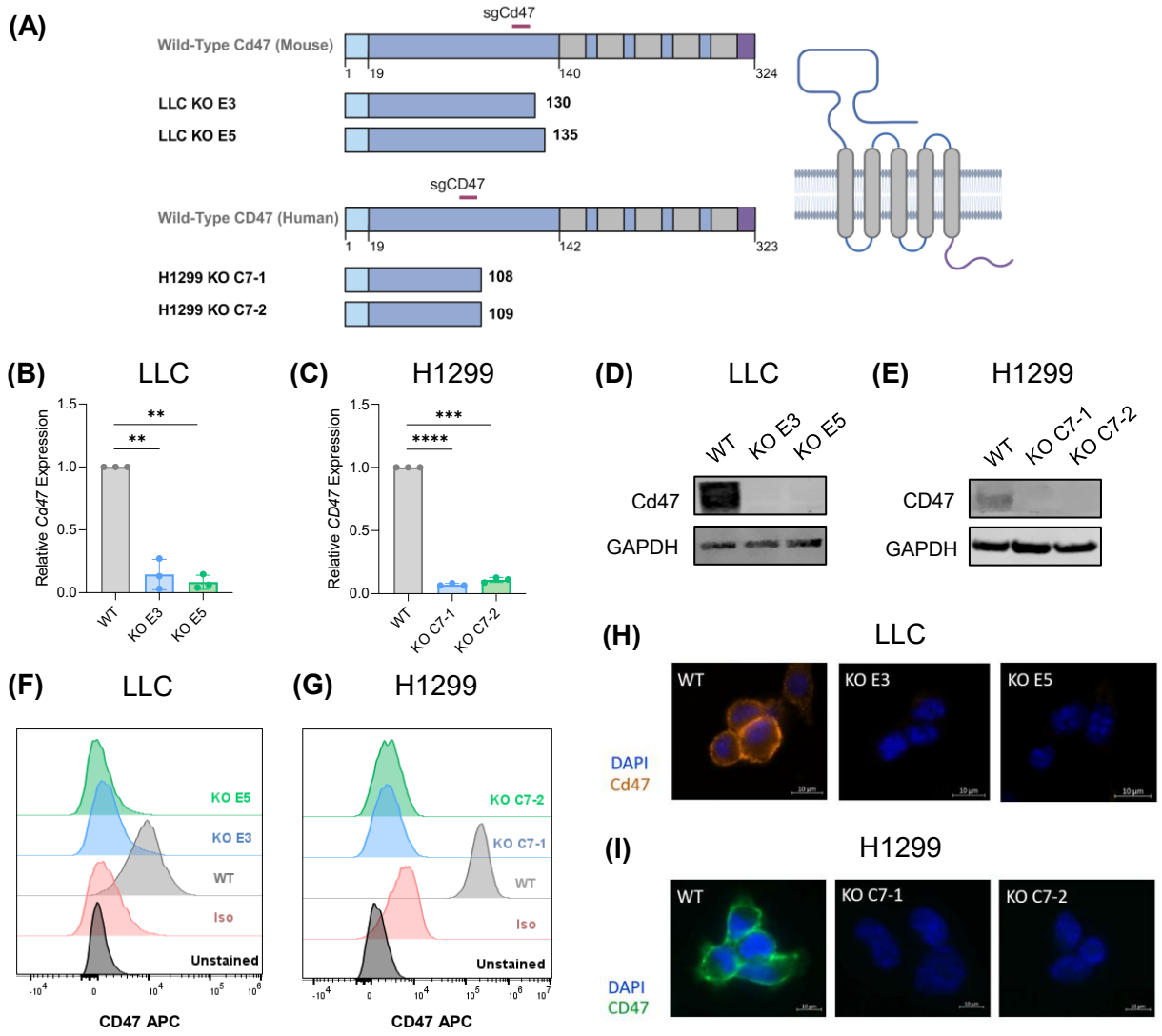
(A)
sgCd47
Wild-Type Cd47 (Mouse)
1
19
140
324
LLC KO E3
130
LLC KO E5
135
sgCD47
Wild-Type CD47 (Human)
1
19
142
323
H1299 KO C7-1
108
H1299 KO C7-2
109
(B)
LLC
Relative Cd47 Expression
1.5
1.0
0.5
0.0
**
**
WT
KO E3
KO E5
(C)
H1299
Relative CD47 Expression
1.5
1.0
0.5
0.0
***
****
WT
KO C7-1
KO C7-2
(D)
LLC
WT
KO E3
KO E5
Cd47
GAPDH
(E)
H1299
WT
KO C7-1
KO C7-2
CD47
GAPDH
(F)
LLC
KO E5
KO E3
WT
Iso
Unstained
CD47 APC
(G)
H1299
KO C7-2
KO C7-1
WT
Iso
Unstained
CD47 APC
(H)
LLC
WT
KO E3
KO E5
DAPI
Cd47
(I)
H1299
WT
KO C7-1
KO C7-2
DAPI
CD47

Figure.2

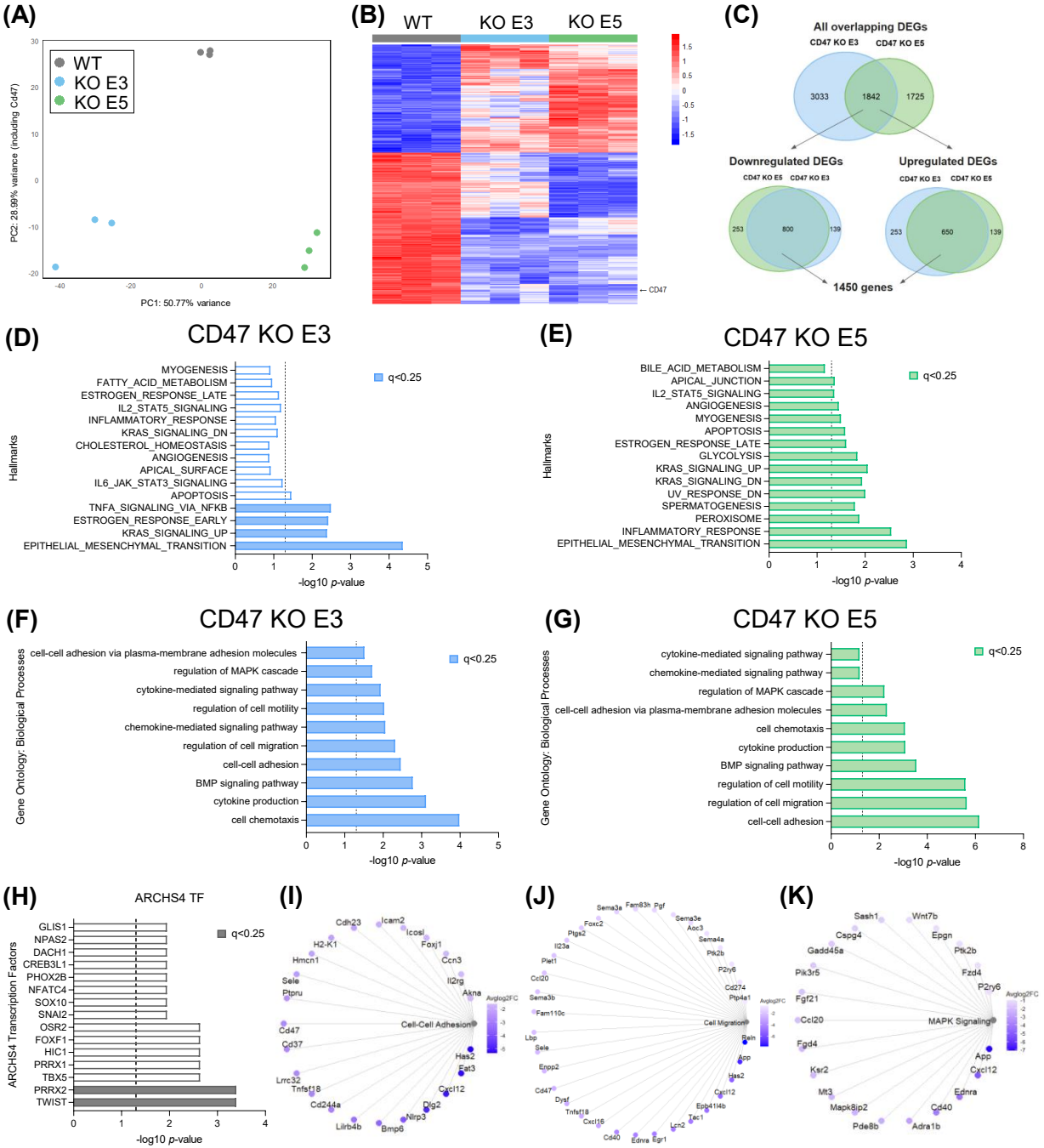
(A)
WT
KO E3
KO E5
PC2: 28.99% variance (including Cd47)
PC1: 50.77% variance
(B)
WT
KO E3
KO E5
CD47
(C)
All overlapping DEGs
CD47 KO E3
CD47 KO E5
3033
1842
1725
Downregulated DEGs
CD47 KO E5
CD47 KO E3
253
800
139
Upregulated DEGs
CD47 KO E3
CD47 KO E5
253
650
139
1450 genes
(D)
CD47 KO E3
q<0.25
Hallmarks
MYOGENESIS
FATTY_ACID_METABOLISM
ESTROGEN_RESPONSE_LATE
IL2_STAT5_SIGNALING
INFLAMMATORY_RESPONSE
KRAS_SIGNALING_DN
CHOLESTEROL_HOMEOSTASIS
ANGIOGENESIS
APICAL_SURFACE
IL6_JAK_STAT3_SIGNALING
APOPTOSIS
TNFA_SIGNALING_VIA_NFKB
ESTROGEN_RESPONSE_EARLY
KRAS_SIGNALING_UP
EPITHELIAL_MESENCHYMAL_TRANSITION
-log10 p-value
(E)
CD47 KO E5
q<0.25
Hallmarks
BILE_ACID_METABOLISM
APICAL_JUNCTION
IL2_STAT5_SIGNALING
ANGIOGENESIS
MYOGENESIS
APOPTOSIS
ESTROGEN_RESPONSE_LATE
GLYCOLYSIS
KRAS_SIGNALING_UP
KRAS_SIGNALING_DN
UV_RESPONSE_DN
SPERMATOGENESIS
PEROXISOME
INFLAMMATORY_RESPONSE
EPITHELIAL_MESENCHYMAL_TRANSITION
-log10 p-value
(F)
CD47 KO E3
q<0.25
Gene Ontology: Biological Processes
cell-cell adhesion via plasma-membrane adhesion molecules
regulation of MAPK cascade
cytokine-mediated signaling pathway
regulation of cell motility
chemokine-mediated signaling pathway
regulation of cell migration
cell-cell adhesion
BMP signaling pathway
cytokine production
cell chemotaxis
-log10 p-value
(G)
CD47 KO E5
q<0.25
Gene Ontology: Biological Processes
cytokine-mediated signaling pathway
chemokine-mediated signaling pathway
regulation of MAPK cascade
cell-cell adhesion via plasma-membrane adhesion molecules
cell chemotaxis
cytokine production
BMP signaling pathway
regulation of cell motility
regulation of cell migration
cell-cell adhesion
-log10 p-value
(H)
ARCHS4 TF
q<0.25
ARCHS4 Transcription Factors
GLIS1
NPAS2
DACH1
CREB3L1
PHOX2B
NFATC4
SOX10
SNAI2
OSR2
FOXF1
HIC1
PRRX1
TBX5
PRRX2
TWIST
-log10 p-value
(I)
Cell-Cell Adhesion
Avglog2FC
(J)
Cell Migration
Avglog2FC
(K)
MAPK Signaling
Avglog2FC

Figure.3

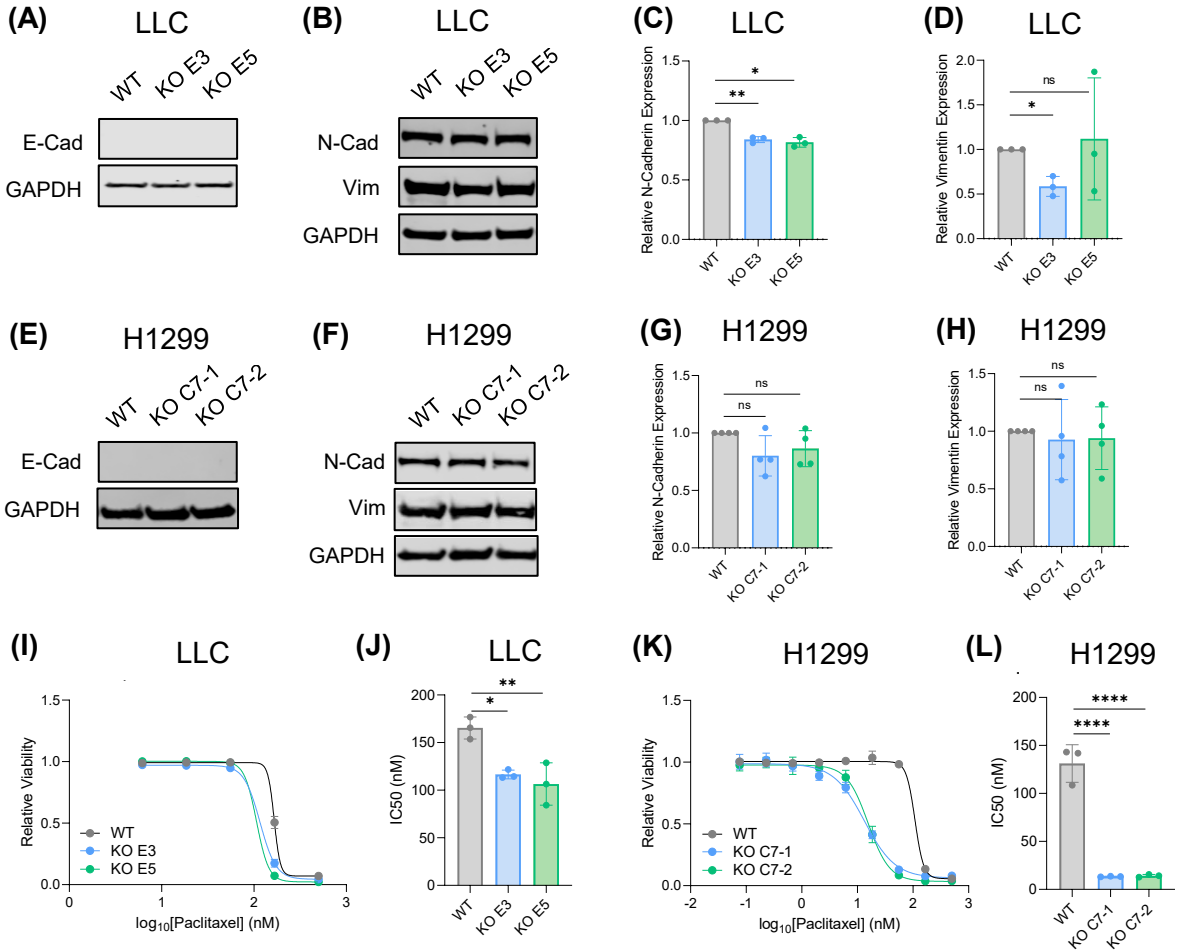
(A)
LLC
WT
KO E3
KO E5
E-Cad
GAPDH
(B)
LLC
WT
KO E3
KO E5
N-Cad
Vim
GAPDH
(C)
LLC
Relative N-Cadherin Expression
1.5
1.0
0.5
0.0
*
**
WT
KO E3
KO E5
(D)
LLC
Relative Vimentin Expression
2.0
1.5
1.0
0.5
0.0
ns
*
WT
KO E3
KO E5
(E)
H1299
WT
KO C7-1
KO C7-2
E-Cad
GAPDH
(F)
H1299
WT
KO C7-1
KO C7-2
N-Cad
Vim
GAPDH
(G)
H1299
Relative N-Cadherin Expression
1.5
1.0
0.5
0.0
ns
ns
WT
KO C7-1
KO C7-2
(H)
H1299
Relative Vimentin Expression
1.5
1.0
0.5
0.0
ns
ns
WT
KO C7-1
KO C7-2
(I)
LLC
Relative Viability
1.5
1.0
0.5
0.0
WT
KO E3
KO E5
0
1
2
3
log10[Paclitaxel] (nM)
(J)
LLC
IC50 (nM)
200
150
100
50
0
**
*
WT
KO E3
KO E5
(K)
H1299
Relative Viability
1.5
1.0
0.5
0.0
WT
KO C7-1
KO C7-2
-2
-1
0
1
2
3
log10[Paclitaxel] (nM)
(L)
H1299
IC50 (nM)
200
150
100
50
0
****
****
WT
KO C7-1
KO C7-2

Figure.4

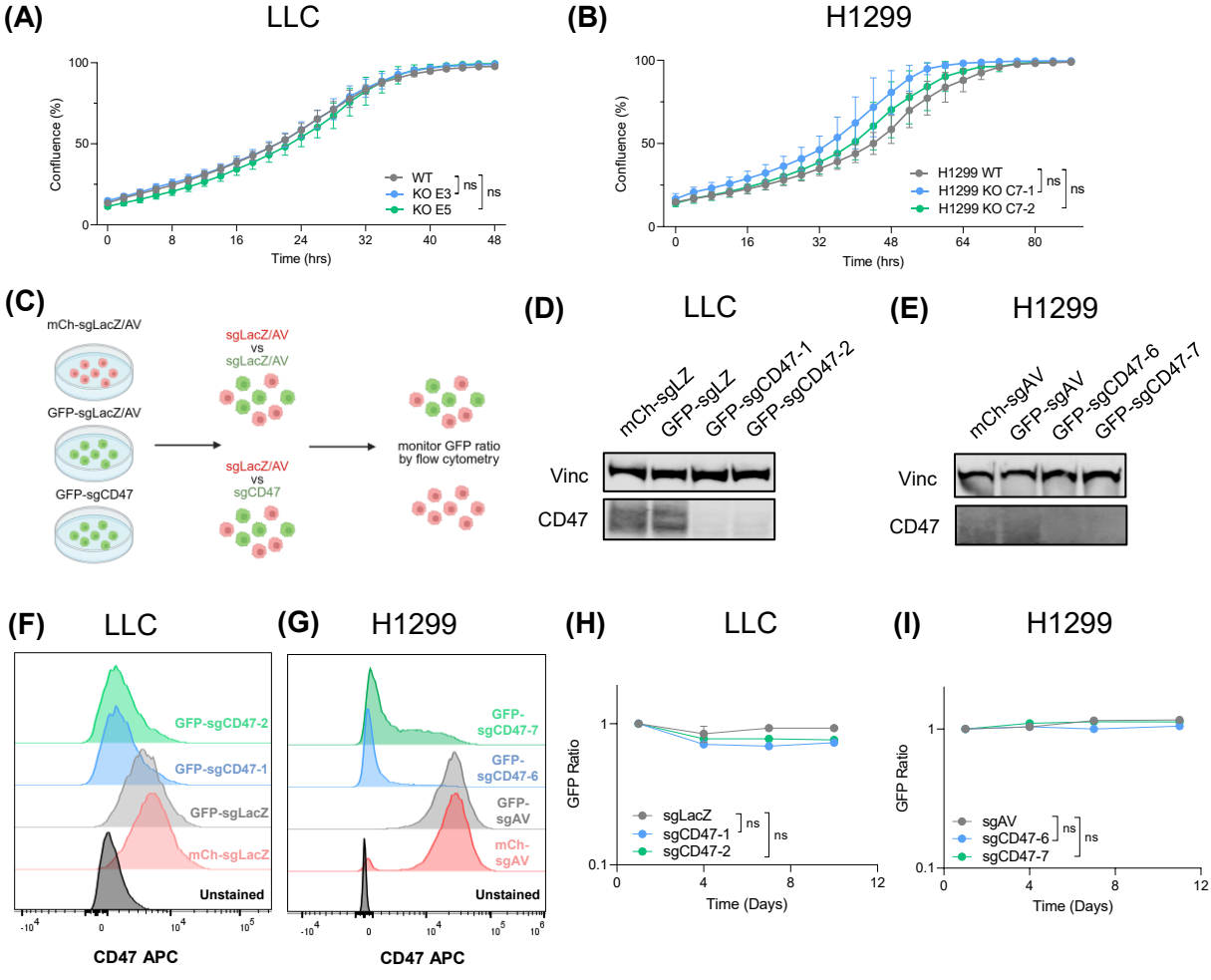
(A)
LLC
Confluence (%)
Time (hrs)
WT
KO E3
KO E5
ns
ns
(B)
H1299
Confluence (%)
Time (hrs)
H1299 WT
H1299 KO C7-1
H1299 KO C7-2
ns
ns
(C)
mCh-sgLacZ/AV
GFP-sgLacZ/AV
GFP-sgCD47
sgLacZ/AV vs sgLacZ/AV
sgLacZ/AV vs sgCD47
monitor GFP ratio by flow cytometry
(D)
LLC
mCh-sgLZ
GFP-sgLZ
GFP-sgCD47-1
GFP-sgCD47-2
Vinc
CD47
(E)
H1299
mCh-sgAV
GFP-sgAV
GFP-sgCD47-6
GFP-sgCD47-7
Vinc
CD47
(F)
LLC
GFP-sgCD47-2
GFP-sgCD47-1
GFP-sgLacZ
mCh-sgLacZ
Unstained
CD47 APC
(G)
H1299
GFP-sgCD47-7
GFP-sgCD47-6
GFP-sgAV
mCh-sgAV
Unstained
CD47 APC
(H)
LLC
GFP Ratio
Time (Days)
sgLacZ
sgCD47-1
sgCD47-2
ns
ns
(I)
H1299
GFP Ratio
Time (Days)
sgAV
sgCD47-6
sgCD47-7
ns
ns

Figure.5

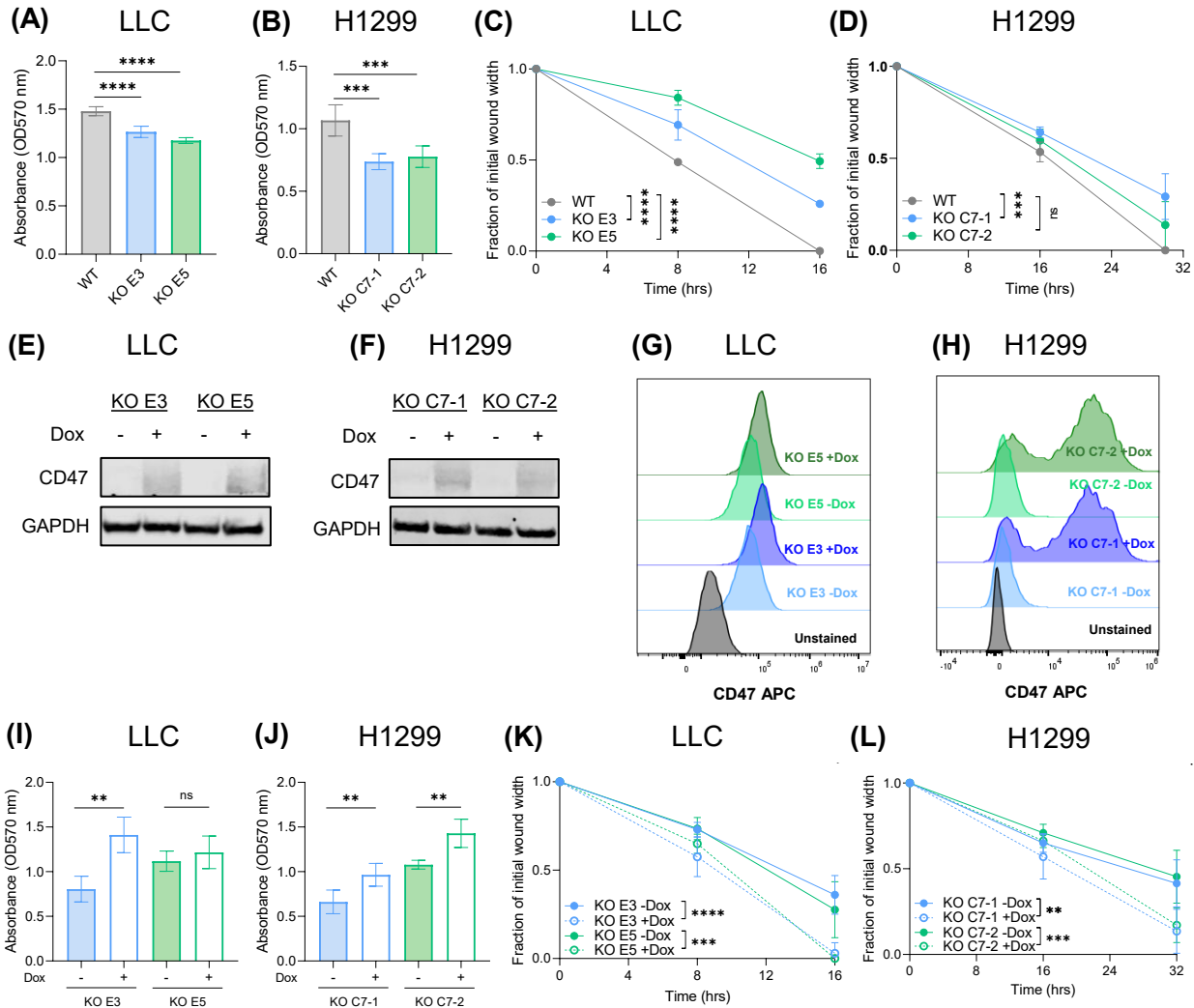
(A) LLC
Absorbance (OD570 nm)
****
****
WT
KO E3
KO E5
(B) H1299
Absorbance (OD570 nm)
***
***
WT
KO C7-1
KO C7-2
(C) LLC
Fraction of initial wound width
WT
KO E3
KO E5
***
****
Time (hrs)
(D) H1299
Fraction of initial wound width
WT
KO C7-1
KO C7-2
***
ns
Time (hrs)
(E) LLC
KO E3
KO E5
Dox
CD47
GAPDH
(F) H1299
KO C7-1
KO C7-2
Dox
CD47
GAPDH
(G) LLC
KO E5 +Dox
KO E5 -Dox
KO E3 +Dox
KO E3 -Dox
Unstained
CD47 APC
(H) H1299
KO C7-2 +Dox
KO C7-2 -Dox
KO C7-1 +Dox
KO C7-1 -Dox
Unstained
CD47 APC
(I) LLC
Absorbance (OD570 nm)
**
ns
Dox
KO E3
KO E5
(J) H1299
Absorbance (OD570 nm)
**
**
Dox
KO C7-1
KO C7-2
(K) LLC
Fraction of initial wound width
KO E3 -Dox
KO E3 +Dox
KO E5 -Dox
KO E5 +Dox
****
***
Time (hrs)
(L) H1299
Fraction of initial wound width
KO C7-1 -Dox
KO C7-1 +Dox
KO C7-2 -Dox
KO C7-2 +Dox
**
***
Time (hrs)

Figure.6

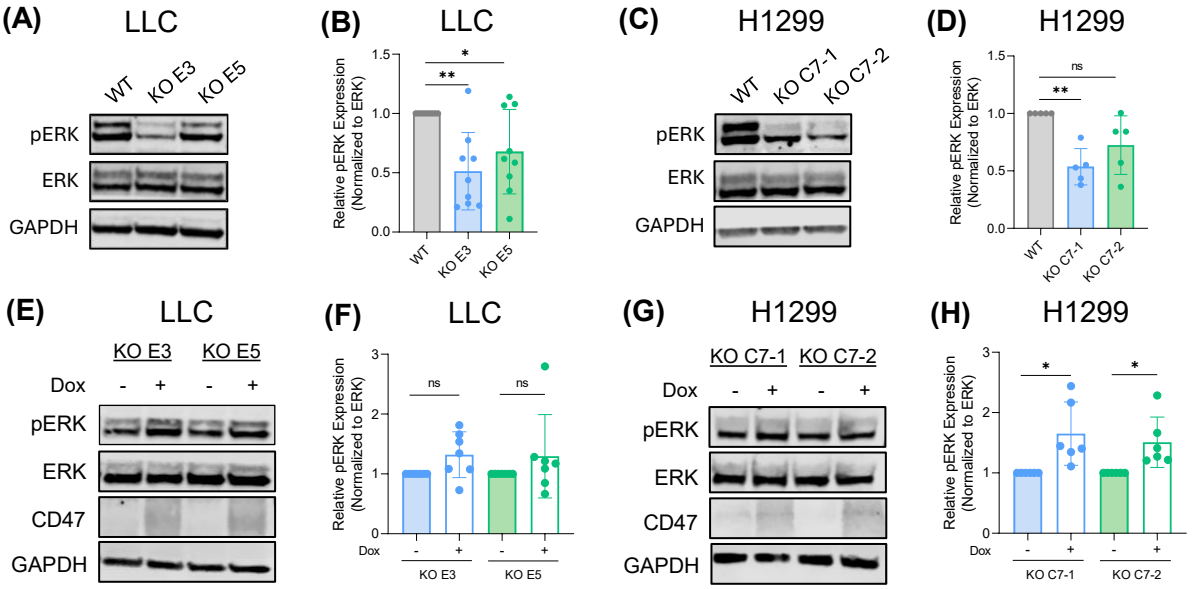
(A)
LLC
WT
KO E3
KO E5
pERK
ERK
GAPDH
(B)
LLC
Relative pERK Expression (Normalized to ERK)
1.5
1.0
0.5
0.0
*
**
WT
KO E3
KO E5
(C)
H1299
WT
KO C7-1
KO C7-2
pERK
ERK
GAPDH
(D)
H1299
Relative pERK Expression (Normalized to ERK)
1.5
1.0
0.5
0.0
ns
**
WT
KO C7-1
KO C7-2
(E)
LLC
KO E3
KO E5
Dox
-
+
-
+
pERK
ERK
CD47
GAPDH
(F)
LLC
Relative pERK Expression (Normalized to ERK)
3
2
1
0
ns
ns
Dox
-
+
-
+
KO E3
KO E5
(G)
H1299
KO C7-1
KO C7-2
Dox
-
+
-
+
pERK
ERK
CD47
GAPDH
(H)
H1299
Relative pERK Expression (Normalized to ERK)
3
2
1
0
*
*
Dox
-
+
-
+
KO C7-1
KO C7-2

Figure.7

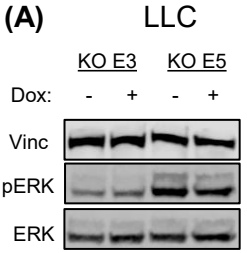
(A)
LLC
KO E3
KO E5
Dox:
-
+
-
+
Vinc
pERK
ERK

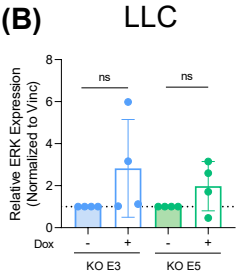
(B)
LLC
Relative ERK Expression
(Normalized to Vinc)
ns
ns
Dox
KO E3
KO E5

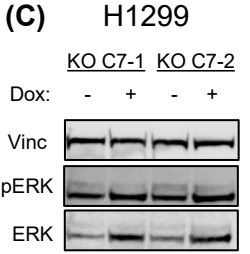
(C)
H1299
KO C7-1
KO C7-2
Dox:
-
+
-
+
Vinc
pERK
ERK

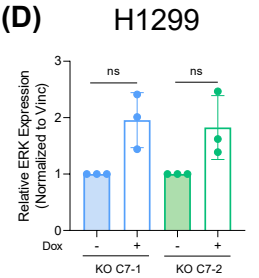
(D)
H1299
Relative ERK Expression
(Normalized to Vinc)
ns
ns
Dox
KO C7-1
KO C7-2

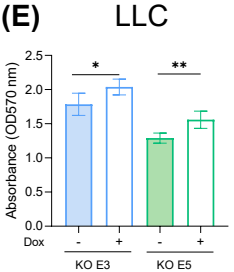
(E)
LLC
Absorbance (OD570 nm)
*
**
Dox
KO E3
KO E5

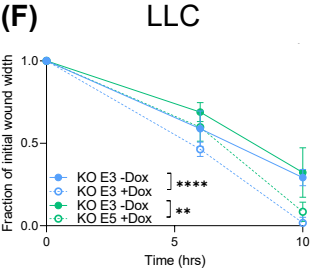
(F)
LLC
Fraction of initial wound width
KO E3 -Dox
KO E3 +Dox
KO E3 -Dox
KO E5 +Dox
****
**
Time (hrs)

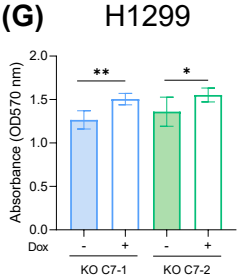
(G)
H1299
Absorbance (OD570 nm)
**
*
Dox
KO C7-1
KO C7-2

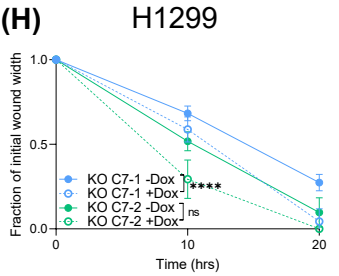
(H)
H1299
Fraction of initial wound width
KO C7-1 -Dox
KO C7-1 +Dox
KO C7-2 -Dox
KO C7-2 +Dox
****
ns
Time (hrs)